Quantifying surface water–groundwater interactions using time series analysis of streambed thermal records: Method development

Christine E. Hatch,[1] Andrew T. Fisher,[1,2] Justin S. Revenaugh,[3] Jim Constantz,[4] and Chris Ruehl[1]

Received 3 December 2005; revised 24 May 2006; accepted 16 June 2006; published 11 October 2006.

[1] We present a method for determining streambed seepage rates using time series thermal data. The new method is based on quantifying changes in phase and amplitude of temperature variations between pairs of subsurface sensors. For a reasonable range of streambed thermal properties and sensor spacings the time series method should allow reliable estimation of seepage rates for a range of at least ±10 m d^{-1} (±1.2 × 10^{-2} m s^{-1}), with amplitude variations being most sensitive at low flow rates and phase variations retaining sensitivity out to much higher rates. Compared to forward modeling, the new method requires less observational data and less setup and data handling and is faster, particularly when interpreting many long data sets. The time series method is insensitive to streambed scour and sedimentation, which allows for application under a wide range of flow conditions and allows time series estimation of variable streambed hydraulic conductivity. This new approach should facilitate wider use of thermal methods and improve understanding of the complex spatial and temporal dynamics of surface water–groundwater interactions.

Citation: Hatch, C. E., A. T. Fisher, J. S. Revenaugh, J. Constantz, and C. Ruehl (2006), Quantifying surface water–groundwater interactions using time series analysis of streambed thermal records: Method development, *Water Resour. Res.*, *42*, W10410, doi:10.1029/2005WR004787.

1. Motivation and Goals

[2] Managing fresh water resources that are increasingly stressed by municipal, agricultural and industrial demands is difficult, particularly because of variations in the hydrologic cycle associated with global and regional climate change [e.g., *Arnell and Liu*, 2001; *Barnett et al.*, 2005; *Bower et al.*, 2004; *Lettenmaier et al.*, 1999; *Panagoulia and Dimou*, 1996; *Snyder et al.*, 2002; *Sophocleous*, 2004]. Discharges in many streams in the western United States have declined during the summer and fall in recent years, when the primary source of stream water is groundwater seepage [*Bachman et al.*, 2005; *Sophocleous*, 2000; *Winter et al.*, 1998], suggesting that some basins have experienced a decrease in surface water–groundwater (SW-GW) exchange. Basin sustainable yield calculations should account for outcomes such as reductions in base flow and changes in groundwater recharge [e.g., *Bredehoeft et al.*, 1982], but measuring these flows is challenging.

[3] "Streambed seepage" refers to the movement of water between the stream channel and streambed; it occurs on many temporal and spatial scales, and is influenced locally and regionally by both natural and anthropogenic processes [e.g., *Chen and Shu*, 2002; *Ruehl et al.*, 2006; *Winter et al.*, 1998; *Woessner*, 2000]. Streambed seepage may contribute to base flow; aquifer recharge, if downward seepage reaches the water table; or hyporheic flow, the movement of stream channel water into the shallow subsurface with subsequent return to the channel and no net change in channel discharge [e.g., *Bencala and Walters*, 1983; *Grimm and Fisher*, 1984; *Malard et al.*, 2002]. Streambed seepage can positively or negatively impact water quality in both streams and aquifers [e.g., *Grasby et al.*, 1999; *Greeff*, 1994; *Valett et al.*, 1996], and may aid stream temperature regulation and nutrient cycling [*Hendricks and White*, 1991; *Petts et al.*, 1999; *Smith*, 1986], both of which are important for aquatic habitat [*Alexander and Caissie*, 2003; *Hayashi and Rosenberry*, 2002; *Power et al.*, 1999].

[4] Numerous methods have been used to assess streambed seepage, including differential gauging, seepage meters, shallow piezometers, and tracer injection experiments [e.g., *Lee and Cherry*, 1978; *Rosenberry and Morin*, 2004; *Bencala et al.*, 1990; *Clark et al.*, 1996; *Constantz et al.*, 2003; *Kilpatrick and Cobb*, 1985; *Leibundgut et al.*, 1993]. Each of these methods has characteristic spatial and temporal scales, assumptions, uncertainties, costs, and limitations (Table 1). In this study we present a method for using

[1]Earth and Planetary Sciences Department, University of California, Santa Cruz, California, USA.
[2]Institute for Geophysics and Planetary Physics, University of California, Santa Cruz, California, USA.
[3]Department of Geology and Geophysics, University of Minnesota, Minneapolis, Minnesota, USA.
[4]U.S. Geological Survey, Menlo Park, California, USA.

0043-1397/06/2005WR004787$09.00

Table 1. Methods for Estimating Streambed Seepage

Method	Spatial Scale	Temporal Scale	Advantages	Disadvantages
Seepage meter	cm^2 to m^2	hours to days (up to months)	direct quantification of seepage rate; inexpensive and easy to deploy multiple times	point measurement (both space and time); errors introduced by improper installation/deployment
Piezometer (head)	cm^2 to m^2	seconds to minutes	simple, accurate assessment of hydraulic gradient	point measurement (both space and time); labor intensive installation
Streambed temperature	cm^2 to m^2	seconds to minutes (up to months)	relatively inexpensive; long thermal records; accurate thermal measurements; can assess seepage rates and directions	point measurement (space); cannot distinguish recharge from subsurface flow
Differential discharge gauging (manual or automated)	10 m^2 to km^2	hours (up to months to years)	measures amount of water in stream directly; simple water mass balance calculation	labor intensive; difficult when flows are low or turbulent; must account separately for ET, in/outflows; requires generation of rating curves at all sites; site maintenance
Tracer injection tests	10 m^2 to km^2	hours to days	can assess flow loss and lateral inflow in an entire reach	cannot distinguish subsurface flow from loss; may be affected by tracer adsorption; point measurement (time)

heat as a seepage tracer. The benefits of using heat as a tracer in groundwater systems have been recognized for decades [e.g., *Bredehoeft and Papadopulos*, 1965; *Mansure and Reiter*, 1979; *Silliman and Booth*, 1993; *Stallman*, 1965; *Taniguchi*, 1993], and there is particular interest in applying thermal methods to assess SW-GW interactions [e.g., *Anderson*, 2005; *Burow et al.*, 2005; *Conant*, 2004; *Constantz and Stonestrom*, 2003; *Constantz et al.*, 1994; *Lapham*, 1989; *Shao et al.*, 1998; *Silliman et al.*, 1995].

[5] Heat is a naturally occurring tracer in stream systems and recent developments in measurement and logger technology have made accurate, reliable data collection both easier and cheaper than in the past. Forward modeling is the most common approach reported in the literature for interpretation of streambed thermal records, and fast computers and widely available models of coupled fluid-heat flow allow quantitative interpretation of these data [e.g., *Bravo et al.*, 2002; *Niswonger and Prudic*, 2003; *Ronan et al.*, 1998]. We develop a new method for interpreting streambed thermal records, based on quantitative relations between the rate and direction of streambed seepage and changes in the phase and amplitude of thermal waves that move from the stream into the streambed.

[6] The new method offers advantages over traditional forward modeling. It requires no information on the absolute depths of temperature sensors, instead relying on the spacing between sensor pairs, making it relatively insensitive to streambed scour or sedimentation. The new method is also faster than traditional forward modeling. The new method does not bypass common limitations of using thermal data to estimate seepage rates, including streambed heterogeneity, finite instrument response time, and the need to know (or estimate) streambed thermal properties; these limitations are addressed later in this paper. The focus of this paper is on method theory, sensitivity, and implementation; later studies will focus on field applications and optimization.

2. Analytical, Numerical, and Field Methods

2.1. Problem Configuration and Governing Equations

[7] For most of this paper we evaluate thermal conditions within a semi-infinite half-space, representing the upper part of the streambed in one dimension (Figure 1). This approach can be extended to two and three dimensions and can incorporate greater geometrical complexity and property heterogeneity (and anisotropy) than shown initially, but the method is best illustrated using simple geometry and property distributions.

[8] Temperature conditions in the half-space are assumed to be governed by a one-dimensional conduction-advection-dispersion equation [e.g., *Anderson*, 2005; *Carslaw and Jaeger*, 1959; *Goto et al.*, 2005; *Stallman*, 1965]:

$$\frac{\partial T}{\partial t} = \kappa_e \frac{\partial^2 T}{\partial z^2} - \frac{n v_f}{\gamma} \frac{\partial T}{\partial z} \tag{1}$$

where T is temperature (varies with time, t, and depth, z), κ_e is effective thermal diffusivity, $\gamma = \rho c / \rho_f c_f$, the ratio of heat capacity of the streambed to the fluid ($\rho_f c_f$ is heat capacity of the fluid, ρc is heat capacity of the saturated sediment-fluid system), n is porosity, and v_f is vertical fluid velocity (positive = up). This formulation can be applied to saturated or unsaturated systems, including systems in which saturation changes with time, using either a fully coupled or partially coupled mathematical representation. In the fully coupled case, changes in temperature and pressure result in modifications to fluid and sediment properties and may lead to convection if represented in two or three dimensions. In the partially coupled case, the fluid velocity

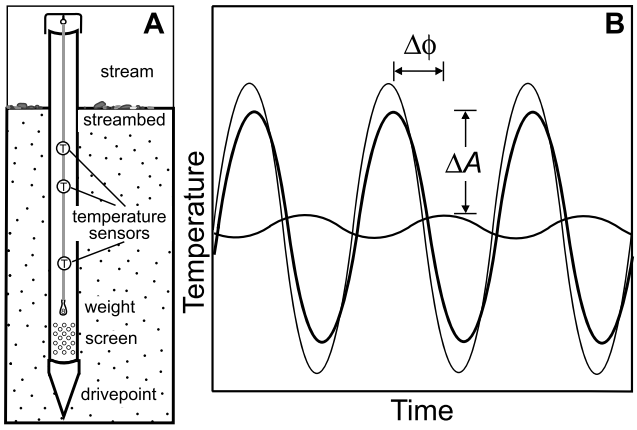

Figure 1. Diagrams illustrating acquisition of streambed temperature records and basis for new analytical method. (a) Streambed piezometer with temperature sensors at various depths. (b) Temperature versus time records showing reduction in amplitude (ΔA) and shift in phase ($\Delta\phi$) with greater depth.

is imposed using fixed or time-variable boundary conditions (Dirichlet or Neumann), and heat transport influences fluid transport only through (generally modest) changes in temperature-dependant hydraulic conductivity. Other bulk properties remain constant or vary with water content, and fluid velocity may vary with depth as fluid moves in and out of storage. For purposes of this study, we assume that the streambed remains fully saturated, but this requirement could be relaxed through modest modification of the analytical method.

[9] The effective thermal diffusivity is defined as [*Ingebritsen and Sanford*, 1998]:

$$\kappa_e = \frac{\lambda_e}{\rho c} = \frac{\lambda_0}{\rho c} + \beta |v_f| \tag{2}$$

where λ_e is the effective thermal conductivity, λ_0 is the baseline thermal conductivity (in the absence of fluid flow), and β is thermal dispersivity. There are several physical rules used to estimate the baseline thermal conductivity of saturated fluid-sediment system, the most common based on geometric mean mixing [e.g., *Brigaud and Vasseur*, 1989; *Horai*, 1971; *Kinoshita*, 1994; *Sass et al.*, 1971; *Woodside and Messmer*, 1961]: $\lambda_0 = \lambda_f^n \lambda_g^{(1-n)}$, where λ_g = grain conductivity.

[10] The second term in equation (2) represents the increase in effective thermal diffusivity caused by hydrodynamic dispersion. The use of dispersion in studies of heat transport by groundwater is inconsistent and somewhat controversial. In models of relatively large systems and modest fluid flow rates, dispersive heat transport is often assumed to be represented by thermal conductivity and/or to have little influence [e.g., *Bear*, 1972; *Woodbury and Smith*, 1985]. Other researchers include dispersion in models and argue for selection of particular values, often by analogy to chemical dispersion and/or based on measurement scale [e.g., *de Marsily*, 1986; *Hopmans et al.*, 2002; *Niswonger and Prudic*, 2003; *Smith and Chapman*, 1983]. As shown later, selection of appropriate thermal dispersivity values is important for correct interpretation of streambed thermal records, whether using the time series method or a forward model.

[11] The solution to equation (1), given periodic variations in temperature at the top of the half-space is (modified from *Goto et al.* [2005] and *Stallman* [1965]):

$$T(z,t) = A \exp\left(\frac{vz}{2\kappa_e} - \frac{z}{2\kappa_e}\sqrt{\frac{\alpha + v^2}{2}}\right) \cos\left(\frac{2\pi t}{P} - \frac{z}{2\kappa_e}\sqrt{\frac{\alpha - v^2}{2}}\right) \tag{3}$$

where A is amplitude of temperature variations at the upper boundary, P is period of temperature variations ($P = 1/f$, f is frequency), and $\alpha = \sqrt{v^4 + (8\pi \cdot \kappa_e/P)^2}$. The rate of penetration of the thermal front (v) is proportional to the fluid velocity: $v = v_f/\gamma$. The first term on the right-hand side of equation (3) defines damping of the amplitude of temperature variations with depth into the streambed, whereas the second term defines the shift in phase with depth.

[12] Thus the predicted temperatures at depth resulting from thermal conduction, advection and dispersion are a nonlinear function of sediment and fluid thermal properties, fluid velocity, and the frequency of surface temperature variations. Higher-frequency temperature variations penetrate more rapidly into the streambed than do lower-frequency variations, but are dampened more abruptly with depth. If there are surface temperature variations having more than one characteristic frequency, these can be summed to predict temperatures at depth, a characteristic of the solution that we exploit.

[13] Equation (3) can be separated into components and solved for the ratio of amplitude variations between pairs of temperature measurement points at different depths ($A_r = A_d/A_s$):

$$A_r = \exp\left\{\frac{1}{2\kappa_{e,d}\kappa_{e,s}}\left[v\left(z_d\kappa_{e,s} - z_s\kappa_{e,d}\right) - \left(z_d\kappa_{e,s}\sqrt{\frac{\alpha_d + v^2}{2}} - z_s\kappa_{e,d}\sqrt{\frac{\alpha_s + v^2}{2}}\right)\right]\right\} \tag{4a}$$

where subscripts s and d refer to effective properties at the shallower and deeper measurement points, respectively. If effective sediment properties between the measurement points are the same as those above the shallower point, equation (4a) reduces to

$$A_r = \exp\left\{\frac{\Delta z}{2\kappa_e}\left(v - \sqrt{\frac{\alpha + v^2}{2}}\right)\right\} \tag{4b}$$

where Δz is the spacing between measurement points. Absolute measurement depths do not appear in equation (4b), meaning that the relations are insensitive to changes in the position of the upper boundary. Streambed scour or deposition does not change this relation, as long as the spacing between sensor pairs remains constant.

[14] Similar relations can be developed for the phase shift between two measurement points ($\Delta\phi$), the time delay

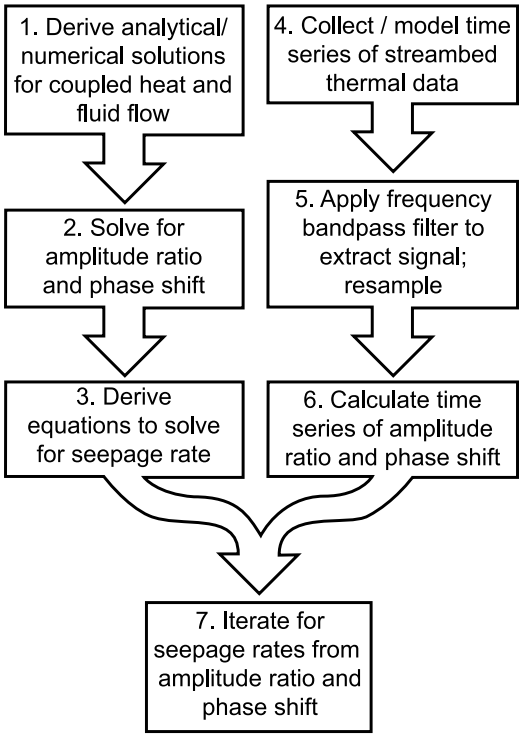

Figure 2. Steps in development and application of time series method. Steps 1–3 provide the theoretical basis for the method (section 2.1), whereas steps 4–7 are required to apply the method to synthetic and field data (sections 2.2 to 3).

between arrival of the peak or trough of a thermal wave at the two depths:

$$\Delta\phi = \frac{P}{4\pi}\left(\frac{z_d}{\kappa_{e,d}}\sqrt{\frac{\alpha_d - \nu^2}{2}} - \frac{z_s}{\kappa_{e,s}}\sqrt{\frac{\alpha_s - \nu^2}{2}}\right) \tag{5a}$$

If effective sediment properties between the measurement points are the same as those above the shallower point, equation (5a) reduces to:

$$\Delta\phi = \frac{P\Delta z}{4\pi\kappa_e}\sqrt{\frac{\alpha - \nu^2}{2}} \tag{5b}$$

Equations (4b) and (5b) are rearranged to solve for the velocity of a thermal front as a function of amplitude and phase relations (v_{Ar} and $v_{\Delta\phi}$ respectively):

$$v_{Ar} = \frac{2\kappa_e}{\Delta z}\ln A_r + \sqrt{\frac{\alpha + \nu^2}{2}} \tag{6a}$$

$$v_{\Delta\phi} = \sqrt{\alpha - 2\left(\frac{\Delta\phi 4\pi\kappa_e}{P\Delta z}\right)^2} \tag{6b}$$

Thermal front velocities appear on both sides of equations (6a) and (6b), explicitly and embedded in α, requiring that they be solved iteratively (or by optimization). Once v is determined, fluid velocities may be derived from thermal front velocities by applying the relationship defined earlier: $v_{f,\Delta\phi} = v_{\Delta\phi}\gamma$ and $v_{f,Ar} = v_{Ar}\gamma$. If both equations are applied to data sets from a single pair of sensors, amplitude and phase relations should indicate the same fluid velocities; as a practical matter, the two relations have different sensitivities and limitations.

[15] For a two- or three-dimensional system having a flat upper boundary and an arbitrary fluid flow field, equations (4)–(6) can be used to describe the vertical fluid flow vector component. More complex systems having irregular upper boundary conditions, or variations in properties or fluid flow rate with horizontal position, require numerical analysis to generate relations equivalent to equations (4)–(6). Results from these calculations can then be used with the rest of the time series approach described below to estimate fluid velocities or seepage rates from streambed thermal data.

2.2. Numerical Approximation of Governing Equations

[16] We use VS2DH, a partially coupled model of fluid and heat flow [*Healy*, 1990; *Healy and Ronan*, 1996; *Hsieh et al.*, 2000], to create synthetic data sets based on stream temperature observations having greater complexity than is possible with analytical solutions, evaluate sensitivity to parameter selection, and quantify uncertainties. We run simulations using a one-dimensional domain comprising the upper 4 m of a streambed, a thickness significantly greater than the interval ($\leq$1 m) that provides the most useful information for the range of properties and flow rates tested. Node spacing and time steps are made small enough ($\geq$0.1 mm, 9 s) so as to allow replication of analytical solutions within resolution of the data loggers and sampling intervals typically used in field studies.

[17] The upper boundary of the grid is assigned a variety of temperature-time histories, depending on the goal of individual simulations, whereas the lower boundary is assigned either a constant temperature equal to the mean of that at the upper boundary, or a polynomial fit to the temperature-time history (essentially a low-pass filtered stream record). In some simulations, we use a simple sinusoid for the upper boundary temperature, allowing direct comparison between numerical and analytical solutions. This is particularly useful in testing data handling and processing tools, to verify that filtering does not introduce spurious frequencies or degrade desired signals. In other simulations, temperature variations having multiple frequencies are used; these are synthetic records composed of a sum of multiple sinusoids, or field records of stream temperatures containing a rich variety of frequency and amplitude information. Fluid is forced to flow through the model domain at rates determined by heads imposed at the upper and lower boundaries, sometimes held constant through a simulation, sometimes varied to force changes in fluid velocity with time. Sediment fluid and heat flow and storage properties are varied for individual simulations and experiments. Model output is reformatted to resemble field data and processed using the same methods (Figure 2).

2.3. Typical Field Instrumentation

[18] This paper focuses on method development, but limited field observations are used to generate synthetic data and evaluate method sensitivity and applicability. Subsurface thermal data are collected with instruments hung

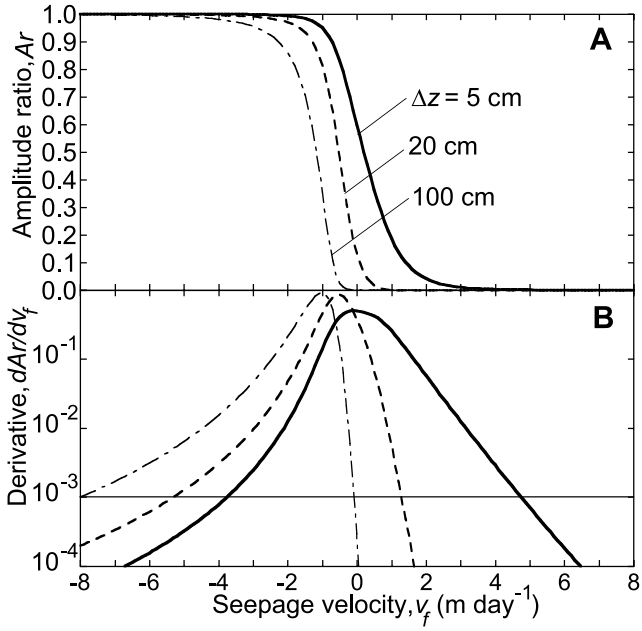

Figure 3. Type curves showing relations between the amplitude of temperature variations as a function of fluid seepage rates for different streambed measurement spacings, Δz. (a) Amplitude ratio, A_r, versus seepage velocity, where $A_r = A_d/A_s$, A_d is amplitude of variations at the deeper of two depths, and A_s is amplitude at a shallower depth. (b) Derivatives of curves shown in Figure 3a, illustrating peaks in sensitivity at relatively low flows. Derivative curves are asymmetric; specific curve shape depends on sensor spacing and other system properties, as do the seepage velocity corresponding to peak sensitivity and the quantifiable range of seepage rates (interpreted to be those for which $dA_r/dv_f \geq 0.001$ d m^{-1}, indicated with horizontal line).

in piezometers driven into a streambed. Piezometers are made from schedule-40 poly vinyl chloride (PVC) having an inner diameter of 3.2 cm (1–¼ in), tipped with a steel drive point below a short section of screen, and penetrating 1–2 m below the base of the stream (Figure 1). The small screen above the drive point keeps the piezometer filled with water, helping to maintain good thermal contact between the sensors and piezometer wall. Because temperature sensors used in this study (and commonly available commercially) have a characteristic response time of 3–4 min, data were recorded at 15 min intervals, with nominal resolution and accuracy of 0.15°C (Onset Stowaway and Hobo Tidbit models) or 0.02°C (Onset WaterTemp Pro model). Instrument resolution and accuracy were quantified prior to deployment using a stable, stirred water calibration bath monitored with a reference sensor having resolution and accuracy of 0.002°–0.003°C. The influence of instrument resolution, accuracy, sample interval, and instrument thermal response times are discussed later, and sample field data are shown briefly to illustrate application of the analytical method and computational tools.

2.4. Time Series Analysis and Interpretation of Synthetic and Field Data

[19] Field data contain numerous frequencies of temperature variations, but we wish to work with a single frequency having a large amplitude. We select the frequency with the strongest signal, generally the $f = 1$ d^{-1} (diurnal) frequency, applying a band-pass filter to synthetic and field data to isolate the desired signal(s). The time series method can be applied to essentially any frequency of interest, or to multiple frequencies, but there are practical limits to the usefulness of particular frequencies. Higher-frequency signals generally have smaller amplitudes and will not penetrate as far before being damped below instrument resolution. In addition, signals having periods ($1/f$) shorter than several times the thermal response time of the data logger inside the piezometer are poorly resolved. Lower-frequency signals (weekly, seasonal) may be larger in magnitude but require commensurately longer data records and will result in seepage estimates having lower temporal resolution. In addition to being several times typical instrument response time, a sample time interval of 15 min is many times greater than the Nyquist frequency for the 1 day period, and is therefore sufficient to accurately characterize the desired signal.

[20] Filtered observations (field data or modeled) collected simultaneously from two depths are passed through a program that allows graphically interactive selection of initial peaks, followed by automated picking of subsequent peaks across the remaining records (Figure 2). Individual peaks are matched between the two records, and the amplitude ratio and phase shift are calculated at the targeted frequency (e.g., if data are filtered to extract a frequency of 1 d^{-1}, $\Delta\phi$ and A_r are calculated at $f = 1$ d^{-1}). Resulting data sets of $\Delta\phi$ and A_r versus time are used to calculate thermal front and fluid velocities based on equations (6a) and (6b).

[21] Each pair of temperature loggers allows seepage rate to be calculated twice (using amplitude ratio and phase shift) at the selected frequency. Thus an array of N streambed temperature loggers may allow as many as $2 \times (N-1)!$ quasi-independent calculations of seepage rate per period. However, as shown later, amplitude and phase relations are most useful for selected ranges of flow rates and directions, and the utility of different sensor spacings depends on signal frequency and amplitude and sediment-fluid thermal properties.

3. Analytical and Numerical Results

3.1. Analytical Relations

[22] Equations (4b) and (5b) define type curves relating amplitude ratio (A_r) and phase shift ($\Delta\phi$) between pairs of measurement points (Δz) to the magnitude and direction of vertical streambed seepage. A_r versus v_f curves are monotonic and asymmetric (Figure 3). More rapid downward seepage results in higher A_r values, as does closer sensor spacing. More rapid upward seepage results in lower A_r values, as does greater sensor spacing. The shapes of the A_r versus v_f curves vary for different instrument spacing, a pattern expressed most clearly in a plot of dA_r/dv_f derivatives (Figure 3b). In general, there is greater sensitivity at relatively low flow velocities (when conduction becomes more important relative to advection), but peak sensitivity depends on measurement spacing and sediment-fluid thermal properties. For the measurement spacings and properties included in this analysis, the amplitude ratio is most useful for estimating

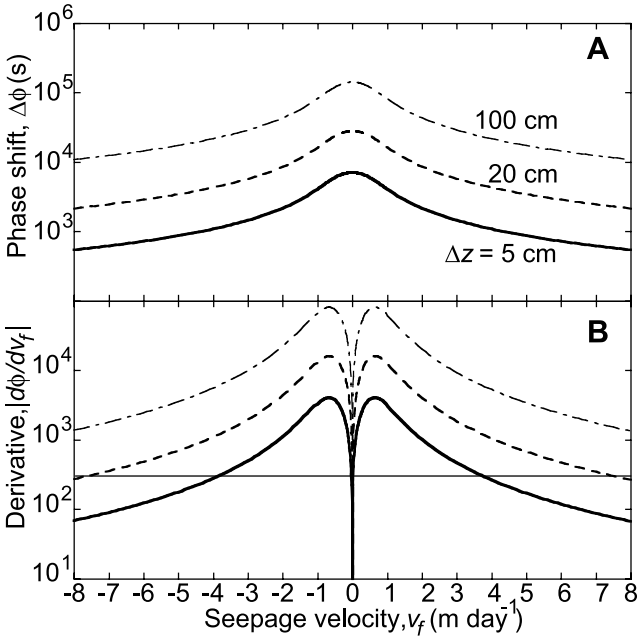

Figure 4. Type curves showing relations between the phase of temperature variations as a function of fluid seepage rates for different streambed measurement spacings, Δz. (a) Phase shift, $\Delta\phi$, versus seepage velocity. (b) Derivatives of curves shown in Figure 4a, illustrating lack of sensitivity at very low seepage velocities and peak sensitivity near ± 1 m d^{-1}. Sensitivity of $\Delta\phi$ remains sufficient to resolve differences in flow rate at higher rates than can be resolved with A_r (Figure 4b). For the present study, derivative values $d\Delta\phi/dv_f \geq 300$ s day m^{-1} (horizontal line) are considered high enough for estimation of seepage rates from observed values of $\Delta\phi$.

seepage rates within a range of -5 to 3 m d^{-1} (-5.8×10^{-5} to 2.7×10^{-5} m s^{-1}).

[23] In contrast, $\Delta\phi$ versus v_f curves are symmetric about zero flow (fully conductive conditions), and thus can be used to estimate fluid flow rate but not direction (Figure 4). This behavior is a direct consequence of velocity appearing in equation (6b) under a square root sign. Also unlike the A_r curves, all $\Delta\phi$ curves reach peak response under purely conductive conditions, where they are least sensitive to changes in seepage rate (Figure 4). For typical physical parameters, the greatest sensitivity of $\Delta\phi$ to seepage rate occurs near ± 1 m d^{-1} ($\pm 1.2 \times 10^{-5}$ m s^{-1}), but sensitivity remains high to greater flow rates than for A_r. Depending on streambed thermal properties and sensor spacing, $\Delta\phi$ values should allow calculation of seepage rates for the range of ± 10 m d^{-1} ($\pm 1.2 \times 10^{-4}$ m s^{-1}); quantification at higher rates will be possible in many cases (Figure 4).

[24] Additional practical limits on application of the time series method are set by the magnitude of stream and streambed temperature variations, instrument resolution and response time, sensor spacing (Figure 5) and sample time interval (Figure 6). Some of these parameters may change little over time (i.e., sediment and fluid thermal properties, if conditions remain saturated), whereas others may vary significantly. Although the governing equations are cast in terms of measurement spacing rather than absolute depth, deeper sensor pairs may fail to provide sufficient signal if the amplitude of surface temperature variations is too small. Also, the most useful measurement spacing varies with seepage rate and direction, both of which may change with time. In the absence of advance knowledge about the rates and directions of flow, or the magnitude of stream temperature variations, it is necessary to deploy sensors at multiple depths (and output model data from a range of depths) so as to have flexibility in data analysis.

[25] For the purposes of the present study, we estimate seepage rates only for values of $dA_r/dv_f \geq 0.001$ (Figure 3b). Where $dA_r/dv_f < 0.001$, at high absolute flow rates, A_r versus v_f curves become flat and small errors in A_r can lead to large errors in estimated seepage rate. During data processing, low dA_r/dv_f values are flagged, and the seepage rate at the derivative limit is assigned (Figure 5). In this case the estimated seepage direction will be correct, but there is only a lower bound on the seepage magnitude.

[26] Similarly for $\Delta\phi$ relations, the method is insensitive to incremental changes in $\Delta\phi$ where type curves are flat (close to zero flow). We limit application of $\Delta\phi$ versus v_f relations to conditions when $d\Delta\phi/dv_f \geq 300$ (Figure 4b), and when $\Delta\phi$ is greater than half the sample time interval (Figure 6). Decreasing sample time interval may yield greater temporal resolution, but would provide little practical benefit because of the finite response time of many field instruments. Instead, we resample filtered temperature records in the frequency domain down to an effective interval of 1 minute to improve accuracy in the identification of both amplitude reduction and phase shift. Calculated $\Delta\phi$ versus v_f relations are most useful at relatively high seepage rates and for sensor spacings <1 m; in contrast, A_r relations are more sensitive at lower rates and greater sensor spacing. The $\Delta\phi$ versus v_f relations provide only the seepage magnitude, not the direction, but the latter is provided by the A_r values, even when the data fall outside

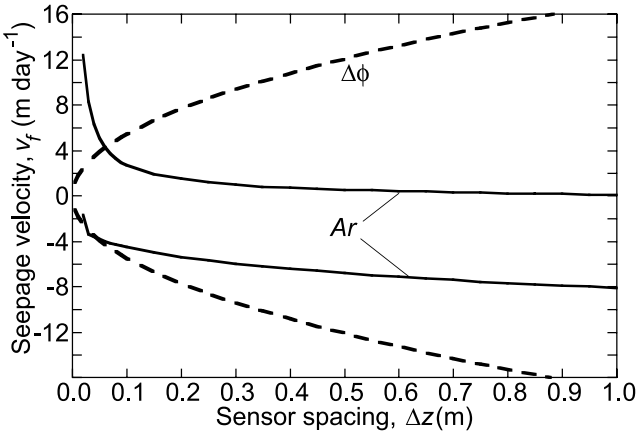

Figure 5. Upper and lower limits on fluid seepage velocities, v_f, that can be calculated from the observed amplitude ratio, A_r, and phase shift, $\Delta\phi$, for a range of sensor spacings, Δz, for $\lambda_0 = 1$ W m^{-1} °C^{-1}, $\beta = 10^{-3}$ m, period, $P = 1$ day, and derivative limits for the present study: $dA_r/dv_f \geq 0.001$ day m^{-1} and $d\Delta\phi/dv_f \geq 300$ s day m^{-1}.

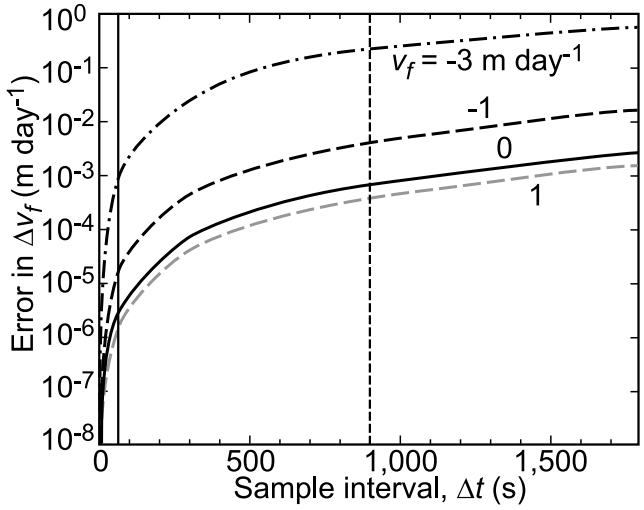

Figure 6. Difference between calculated and correct fluid seepage velocities, Δv_f, as a result of using a finite sample interval, Δt, for Δz = 5 cm, λ_0 = 1 W m^{-1} °C^{-1}, and β = 10^{-3} m. Vertical lines indicate the field sample and postfilter resample intervals for this study: Δt = 900 s (field, dashed line) and Δt = 60 s (resampled, solid line), respectively. Errors are smaller for greater sensor spacings.

the usable A_r range: $A_r \rightarrow 1$ for rapid flow down, $A_r \rightarrow 0$ for rapid flow up (Figure 3).

3.2. Sensitivity to Streambed Thermal Properties

[27] Determining accurate seepage rates using thermal data requires correct streambed thermal conductivity and dispersivity values, but few studies have attempted to determine them directly or explored the sensitivity of interpretations to parameter selection. We evaluate the influence of selecting appropriate values for these parameters by forward calculating the thermal response to streambed seepage using one set of values (creating synthetic observational data), then interpreting the results using different streambed properties. Uncertainties in seepage rates derived from these sensitivity analyses are tabulated and reported (Table 2).

[28] The saturated thermal conductivity of sediments commonly found in streambeds should be in the range of 0.8 to 2.5 W m^{-1} °C^{-1} [e.g., *Hopmans et al.*, 2002; *Kinoshita*, 1994; *Stonestrom and Blasch*, 2003]. Sediments recovered from the field site that generated the data shown later in this paper are predominantly sandy silt, sandy clay, and silty clay [*Goetz*, 2004]; on this basis, we assume a baseline sediment thermal conductivity for illustration purposes of λ_0 = 1 W m^{-1} °C^{-1}. Errors in assumed streambed thermal conductivity may lead to overestimates or underestimates of seepage velocities, depending on the seepage direction and magnitude (Figure 7). Both $\Delta\phi$ and A_r are less influenced by errors in thermal conductivity at higher flow rates, as expected when advection becomes more important for heat transport.

[29] The thermal dispersivity of streambed sediments, and aquifer materials in general, is more difficult to quantify and has greater uncertainty than thermal conductivity. The few quantitative field and lab studies addressing this topic suggest that values similar to chemical dispersivities may be appropriate [e.g., *Barlow*, 1987; *de Marsily*, 1986; *Hopmans et al.*, 2002]. Chemical dispersivity is generally considered to be a parameterization of complex processes and is widely thought to be scale dependant [e.g., *Dagan*, 1984; *Gelhar et al.*, 1992; *Gillham et al.*, 1984; *Neuman*, 1990; *Neuman*, 1995; *Sudicky et al.*, 1983]. The length scales of modeling and field measurements in the present study, based on spacing between sensor pairs used to estimate seepage rates, are 0.05–1.0 m. Assuming that thermal dispersivities are similar in magnitude to chemical dispersivities, standard relations suggest that $\beta \sim 10^{-3}$ m [e.g., *Gelhar et al.*,

Table 2. Comparison of Uncertainty and/or Error in Seepage Rates From Sensitivity Analyses[a]

Parameter	Range(s) of Parameters Explored		Uncertainty or Error in Seepage Velocities	
	Δz, m	Δt,[b] s	$\Delta v_{f,\ Ar}$,[c] m d^{-1}	$\Delta v_{f,\ \Delta\phi}$,[c] m d^{-1}
Filtering[d]	0.05 to 0.40	60	1.3×10^{-4} to 4.1×10^{-3}	2.5×10^{-3} to 0.16
Thermal conductivity λ[e]	0.05 to 1.00	NA	0.22	0.21
Thermal diffusivity β[f]	0.05 to 1.00	NA	9.8×10^{-3} to 0.38	4.2×10^{-3} to 0.28
Sample interval Δt[g]	0.05	6 to 1800	1.9×10^{-7} to 9.5×10^{-2}	9.3×10^{-4} to 0.25
Numerical model (sinusoid)[h]	0.05 to 0.95	60	1.0×10^{-2} to 1.5×10^{-2}	1.8×10^{-3} to 2.0×10^{-2}
Numerical model (stream temperature)[i]	0.05 to 0.95	60	3.6×10^{-3} to 3.0×10^{-2}	1.8×10^{-3} to 4.0×10^{-2}

[a]Uncertainties in seepage rates were derived from amplitude ratios ($\Delta \boldsymbol{v}_{f,\ Ar}$) and phase shifts ($\Delta \boldsymbol{v}_{f,\ \Delta\phi}$) quantified on the basis of a modeled system for which $v_f = -1$ m d^{-1} (downward seepage), λ_0 = 1 W m^{-1} °C^{-1}, β = 0.001 m, Δt = 60 s, and Δz = 0.05–1.0 m. For each listed parameter a range of values was tested, yielding the uncertainties indicated above.

[b]Sample interval is resampled value where applicable. Field stream temperature data were collected at Δt = 900s, and λ and β tests utilized A_r and $\Delta\phi$ information directly, so Δt is not applicable (NA).

[c]Differences between analytically calculated fluid seepage velocities and those derived using the methods described herein are based on amplitude ratio ($\Delta \boldsymbol{v}_{f,\ Ar}$) and phase shift ($\Delta \boldsymbol{v}_{f,\ \Delta\phi}$) for parameter variations listed.

[d]Neglects edge effects.

[e]Data calculated with thermal conductivity λ = 1 W m^{-1} °C^{-1} and seepage rates interpreted as if λ = 2 W m^{-1} °C^{-1}.

[f]Data calculated with thermal diffusivity β = 0.001 m and seepage rates interpreted as if β = 0 and β = 0.05 m, respectively.

[g]Sample interval tests were also conducted for Δz = 0.1, 0.2, 0.4 and 1.0 m with similar results.

[h]Data calculated with numerical model VS2DH [*Healy*, 1990; *Healy and Ronan*, 1996], driven with a perfect sinusoidal upper boundary.

[i]Data calculated with numerical model VS2DH [*Healy*, 1990; *Healy and Ronan*, 1996]; upper boundary is real stream temperature data.

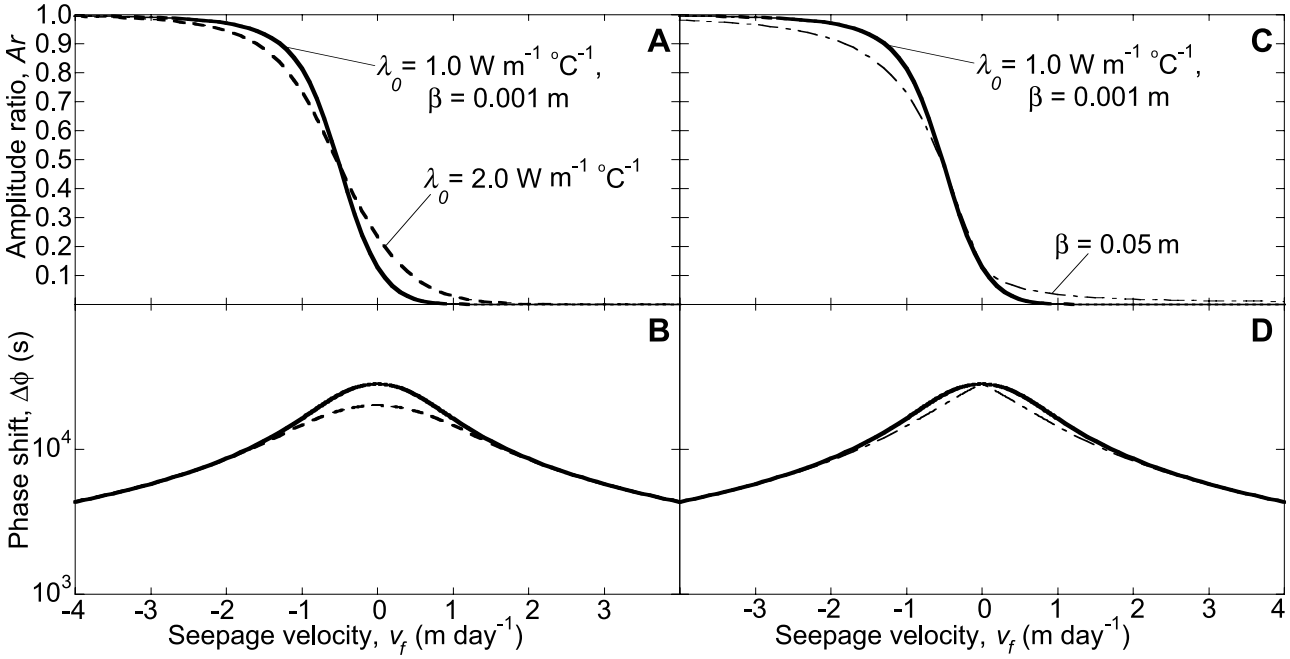

Figure 7. Changes in v_f type curves (Figures 3 and 4) relative to a reference case with $\lambda_0 = 1.0$ W m^{-1} °C^{-1} and $\beta = 0.001$ m (solid line). (a) Variations in amplitude ratio, A_r, when $\lambda_0 = 2.0$ W m^{-1} °C^{-1}. (b) Variations in phase shift, $\Delta\phi$, when $\lambda_0 = 2.0$ W m^{-1} °C^{-1}. (c) Variations in A_r when $\beta = 0.05$ m. (d) Variations in $\Delta\phi$ when $\beta = 0.05$ m.

1992; *Neuman*, 1990, 1995; *Xu and Eckstein*, 1995], as used for most analyses in the present study. As for thermal conductivity, selection of appropriate values of thermal dispersivity is important for accurate calculation of streambed seepage rates (Figure 7). Unlike thermal conductivity, errors in thermal dispersivity become more important in an absolute sense at higher flow rates, although these errors may be less important in a relative sense.

3.3. Characteristics and Processing of Field and Synthetic Data

[30] Thermal records from streams and streambeds often display temperature variability having a range of frequencies. An example stream temperature record (Pajaro River, central coastal CA) illustrates long-term (seasonal) variability on the order of 5°–10°C and diurnal oscillations on the order of 1°–7°C (Figure 8). A power spectrum of these data shows (as do data from several other streams we have examined) significant energy at $f = 1$ d^{-1}, and smaller peaks at higher frequencies (Figure 9). These higher-frequency peaks result from the representation of an asymmetrical (sawtooth) temperature record with an orthogonal set of cosine functions (Figure 10).

[31] Streambed records generally exhibit power spectra that are similar to those from the stream channel, albeit with lower energy at greater depths, as shallower temperature variations are damped with deeper passage of the thermal wave (Figures 9 and 10). In addition, streambed variations in temperature are delayed in phase behind stream records, and higher-frequency signals tend to be damped out with increasing depth, resulting in more sinusoidal signals.

[32] Although it is possible to pick daily temperature peaks in many raw stream and streambed temperature records, the exact timing and amplitude of these variations is difficult to determine when several frequencies of variability are superimposed and temporal resolution is limited. For the present study we apply a cosine taper band-pass filter to raw records, with an all-pass frequency range of 0.9 d$^{-1} \leq f \leq 1.1$ d^{-1}, and allow no energy to pass for $f <$ 0.6 d^{-1} and $f > 1.4$ d^{-1} (Figure 9). We use a two-pass (forward, backward) filter to avoid introducing spurious phase shifts. We experimented with several filter forms, including those having wider and narrower windows and shoulders, and selected a simple filter that minimized edge effects and leakage and maximized signal preservation.

[33] Filtered stream data allow easier and more accurate analysis of streambed temperature records than do raw

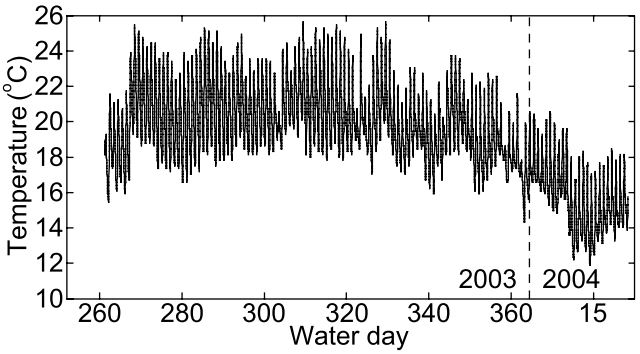

Figure 8. Observed stream temperatures recorded every 15 min late in the 2003 water year (through day 365) and the first part of the 2004 water year in the Pajaro River, central coastal California. Typical diurnal variations are 2°–6°C, superimposed on seasonal variations of 6°–10°C.

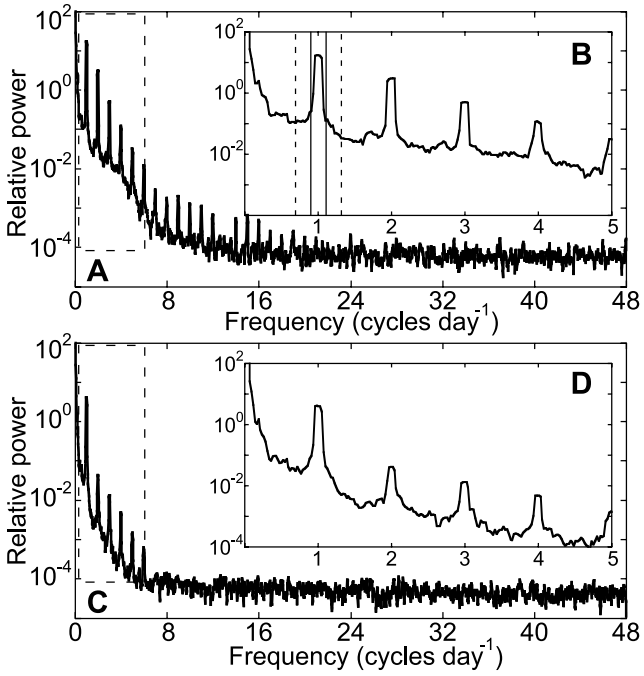

Figure 9. Power spectral density (PSD) analyses of stream and streambed temperature records from the Pajaro River, central coastal California. (a) PSD of stream temperature extending to the Nyquist frequency of 48 cycles d^{-1}. Area in dashed box is shown in Figure 9b. (b) Detail of PSD of stream temperature illustrating strong energy at $f = 1\ d^{-1}$. Limits of the cosine taper window are also shown: all energy is passed between the solid vertical lines, ramping down to no energy being passed outside the dotted vertical lines. (c) PSD of streambed temperature at a nominal depth of 40 cm. Area in dashed box is shown in Figure 9d. (d) Detail of PSD of streambed temperature at $z = 40$ cm. As for stream temperatures, there is strong energy at $f = 1\ d^{-1}$, but higher frequency peaks fall off more rapidly, illustrating filtering by streambed.

records. First, the removal of lower and higher frequencies often reveals temperature oscillations that are not initially apparent or quantifiable in raw data (Figure 11). Second, filtering smoothes data discretization resulting from finite sampling times and instrument resolution (Figures 10b and 11), allowing resampling at a higher frequency than field measurements, and making individual peaks and troughs easier to identify. Filtering imposes edge effects, generally impacting 3–4 days of data at the start and end of each temperature series (Figure 12). For evaluation of diurnal temperature changes, this effect is comparable the time required for a forward model to move beyond the influence of initial conditions.

[34] In summary, processing of streambed temperature data (real and synthetic) follows these steps (Figure 2): Data formats are standardized in individual files, one file for each temperature sensor. The most common sample interval in the present study was 15 min (96 d^{-1}), but more frequent sampling was used in some numerical analyses to minimize discretization errors. Data are filtered, resampled at 1-min intervals, and pairs of filtered data sets are passed to a peak-picking program. This program displays and allows manual (graphical) selection of an initial set of corresponding peaks, then automatically selects subsequent peaks using a local maximum algorithm. The user evaluates, modifies (if necessary), and approves peak selection for the complete data set, and the program calculates and outputs a series of amplitude ratio (A_r) and phase shift ($\Delta\phi$) values, one per day. These values are passed to a program that iterates to determine the apparent seepage rate associated with each A_r and/or $\Delta\phi$ value. Seepage rate based on each A_r value is estimated first to determine if it falls within usable data limits, since A_r relations provide both seepage magnitude and direction and has greater sensitivity at lower rates. If an A_r value falls outside the usable range (generally for very rapid upward or downward flow), the seepage rate based this value is "pegged" at the appropriate limit, and the $\Delta\phi$ value is used to estimate seepage velocity, with the direction based on the results of the A_r analysis.

3.4. Tests of Synthetic Data With Known Seepage Rates

[35] Initial experiments based on sinusoidal surface temperature variations demonstrate that the numerical model replicates analytical solutions (confirming selection of appropriately fine spatial and temporal descretization), and show that filtering does not introduce unacceptable amplitude or phase errors. For example, seepage rate errors no greater than ± 0.02 m d^{-1} are introduced by filtering using modeled data in which the seepage velocity is -1 m d^{-1} (Figure 13a and Table 2).

[36] We create more realistic synthetic temperature records using field data (Figure 8) for the upper thermal boundary condition. Constant and time-varying seepage rates are simulated, and modeled temperature responses at various depths are interpreted using the time series method. For constant seepage rates of ± 1 m d^{-1} errors are ± 0.03 m d^{-1} (Figure 13b and Table 2). As expected, amplitude variations provide more reliable estimates of seepage rates over this range than do variations in phase. Seepage estimates based on synthetic streambed records have somewhat larger errors when seepage rates change (Figure 14). For example, when the seepage rate begins at -0.5 m d^{-1} and ramps to -1.0 m d^{-1} over 15 days, there are short-term increases in error of 0.01–0.03 m d^{-1} for observation depths of $z = 5$ cm and 20 cm below the streambed interface, a spacing of $\Delta z = 15$ cm (Figure 14b). In a simulation in which the seepage rate is initially +0.2 m d^{-1} and ramps down to -0.5 m d^{-1} over 15 days, the largest errors in $v_{f,\,Ar}$ (0.06 m d^{-1}, also for $\Delta z = 15$ cm) occur when the seepage rate changes direction (Figure 14d). Errors are greater when seepage rates change because of the time required for changes in thermal conditions at the surface to propagate to depth. Shallow measurement points respond more rapidly to changes in seepage rate, and thus are more sensitive to transient conditions.

3.5. Field Example

[37] Two months of field data from the Pajaro River (central coastal CA) help to illustrate application of the time series method (Figure 10). Data were collected from a piezometer installed in the center of the stream channel, with sensors at nominal subsurface depths of 10 and 40 cm ($\Delta z = 30$ cm), toward the end of the 2003 water year. Raw

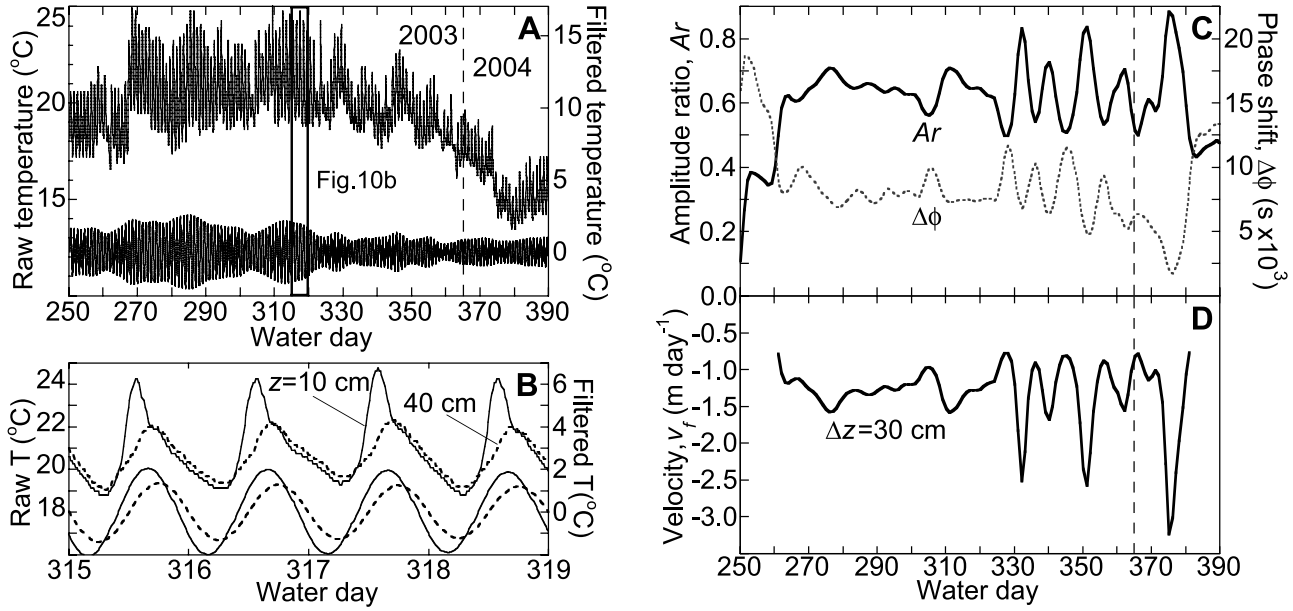

Figure 10. Example stream and streambed temperature records, illustrating time series processing and interpretation steps. (a) Raw (top) and filtered (bottom) temperature records from the Pajaro River, central coastal California. Narrow box indicates part of record shown in Figure 10b. (b) Detail of 4 days of temperature record showing data from z = 10 and 40 cm (Δz = 30 cm). Upper curves are raw data; lower curves are filtered data. The deeper temperature records are shifted in phase and have lower amplitude than the shallower records. (c) Amplitude ratio, A_r, and phase shift, $\Delta\phi$, calculated once per day on the basis of the filtered records. (d) Interpreted streambed seepage velocities based on application of the time series method.

temperature records were filtered and resampled, temperature peaks were picked, A_r and $\Delta\phi$ values were calculated, and seepage rates were estimated by iteration, suggesting seepage velocities of -3.2 to -0.8 m d^{-1} downward (Figure 10). Because calculated seepage rates fall into the range of high A_r sensitivity (Figure 3b), only A_r values are used to estimate seepage rates in this example. The data indicate a mean seepage rate during the period shown of $v_f = -1.3$ m d^{-1}, but the record has two distinct parts defined by variability. The standard deviation of the seepage rate is 0.15 m d^{-1} before water day 320, and 0.6 m d^{-1} during later times. These results are consistent with contemporaneous differential gauging and tracer experiments conducted along the same reach [*Ruehl et al.*, 2006]. Future studies will include processing and interpretation of streambed thermal records from dozens of piezometers installed in this and other stream systems, and comparisons with independent estimates of seepage velocities based on differential gauging, tracer experiments, seepage meters, and shallow head measurements.

4. Discussion

4.1. Errors, Uncertainties, and Limitations

[38] All methods for estimating streambed seepage rates are subject to errors, uncertainties, and limitations (Tables 1 and 2). Random and systematic errors may arise from misapplication of experimental techniques and limitations of field instrumentation. Uncertainties specific to thermal methods arise from spatial heterogeneity and temporal variability, the finite response time of field instruments, and variations in streambed thermal properties. Many of these uncertainties apply to both time series analysis and forward modeling of temperature data, since these approaches are based on the same heat transport physics.

[39] Although the time series approach is based on sensor spacing rather than absolute sensor depths, there are practical limits as to the absolute streambed depth of useful measurements. This maximum depth varies with the seepage direction and rate, requiring that multiple depths be monitored so as to maximize signal strength and minimize noise. In analyses completed thus far, we assume that thermal conductivity and thermal dispersivity are known

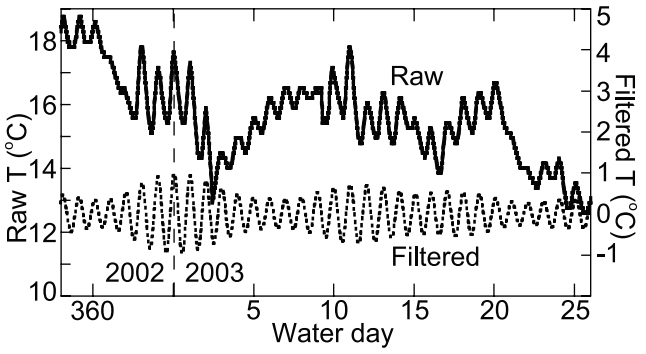

Figure 11. Detail of raw and filtered temperature records illustrating how filtering can reveal diurnal signals that are difficult to resolve in raw records.

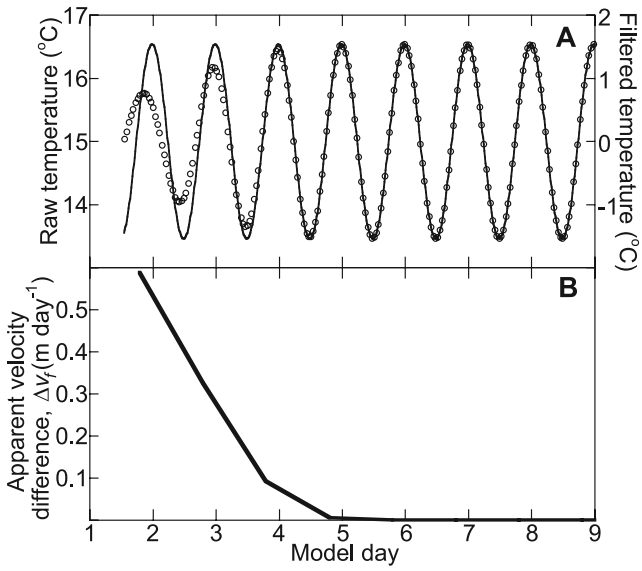

Figure 12. Illustration of edge effects associated with filtering. (a) Raw "data" (solid line) and filtered signal (open circles), based on a perfect sinusoidal of temperature variation at the upper boundary for a system in which the fluid velocity is -1 m d^{-1} (down). Amplitude is reduced near the start of the time series record in the filtered data set. (b) Errors in apparent seepage velocity resulting from edge effect. Errors are relatively large for the first 3–4 days. Similar edge effects occur at the end of a time series record and at the start and end of any data gaps.

through independent analyses or estimates. Misidentification of thermal properties can lead to errors (Figure 8).

[40] The filtering of time series records of streambed temperature introduces edge effects that degrade the first and last 3–4 days of a data series (Figures 12 and 13). Ideally, one measures temperatures for months or more without data gaps, to minimize edge effects. The time series method is sensitive to abrupt changes in seepage rates and directions (Figure 14). This sensitivity results from one of the greatest limitations of using temperature data to assess seepage rates: although there is interest in assessing variations in seepage with time, calculations are often based on a steady state representation of seepage rate (equation (1)). The significance of this limitation depends on the magnitude and frequency of seepage rate variations. Seepage rates in many natural systems will vary continuously and slowly over days to weeks or more, but more rapid changes may occur in systems that are heavily impacted by groundwater pumping, dam releases, or other human activities.

4.2. Method Applicability and Future Work

[41] Although the method developed in this study may seem complex at first, particularly to those unfamiliar with time series analysis, it is simpler and faster to implement than forward modeling. The necessary steps have been implemented using several short MATLAB programs that run quickly and interactively. There are no grids to be generated; property distributions to be assigned; pressure or head data to be collected (in the stream and subsurface), processed, and formatted for model input; or stress periods, time steps or initial conditions to be selected. The time series approach is relatively insensitive to streambed deposition or scour. Although forward models could be set up in a similar fashion, with the upper model boundary at depth, this is not typically done, and would require use of a forward model capable of representing a moving boundary constrained by high-resolution head gradient data. Forward modeling offers some advantages, particularly in cases where there are complex flow geometries or heterogeneous property distributions, but the time series approach can be used to process a large number of long data sets rapidly, helping to select a subset of records for more detailed analysis.

[42] The time series method does not generate direct estimates of streambed hydraulic conductivity, a common goal in forward modeling studies. However, if one collects water level data from the stream and subsurface, these data can be combined with estimates of seepage rate from time series analysis of temperature to estimate streambed hydraulic conductivity versus time. This may prove particularly useful for understanding streambed seepage processes during high-flow conditions, when other approaches for quantifying seepage are difficult to apply. Additional work is underway to test this approach, and to use temperature data collected simultaneously at multiple sensor spacings, at multiple seepage rates, to optimize selection of appropriate thermal properties. Within a system that remains fully saturated, thermal properties should remain constant even

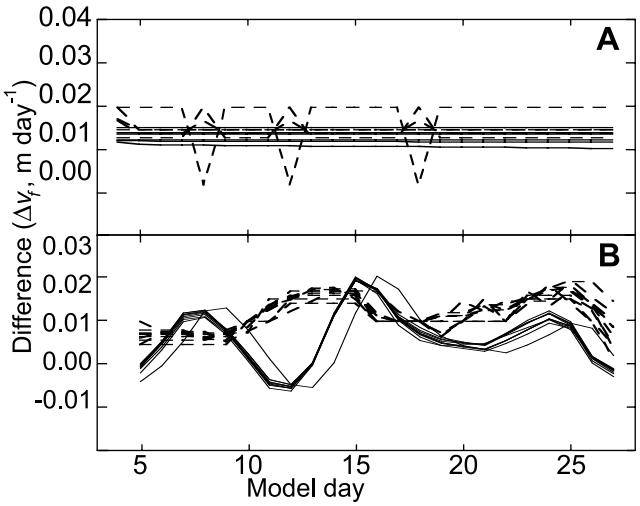

Figure 13. Influence of filtering modeled data on estimated seepage rates based on amplitude ratio, A_r, and phase shift, ϕ, for a range of streambed measurement spacings (5 cm $\leq \Delta z \leq$ 85 cm) and a seepage velocity of $v_f = -1$ m d^{-1}. A perfect sinusoid and stream temperature were used as the upper boundaries for numerical models used to generate synthetic data. After filtering (to allow introduction of associated errors), A_r and ϕ were calculated once per day, then used to determine the seepage rate using equations (6a) and (6b). Solid lines are $\Delta v_{f,Ar}$, and dashed lines are $\Delta v_{f,\Delta\phi}$. (a) Errors, Δv_f, of ±0.02 m d^{-1} for all measurement spacings with a sinusoidal upper boundary and (b) ±0.03 m d^{-1} with a stream temperature upper boundary.

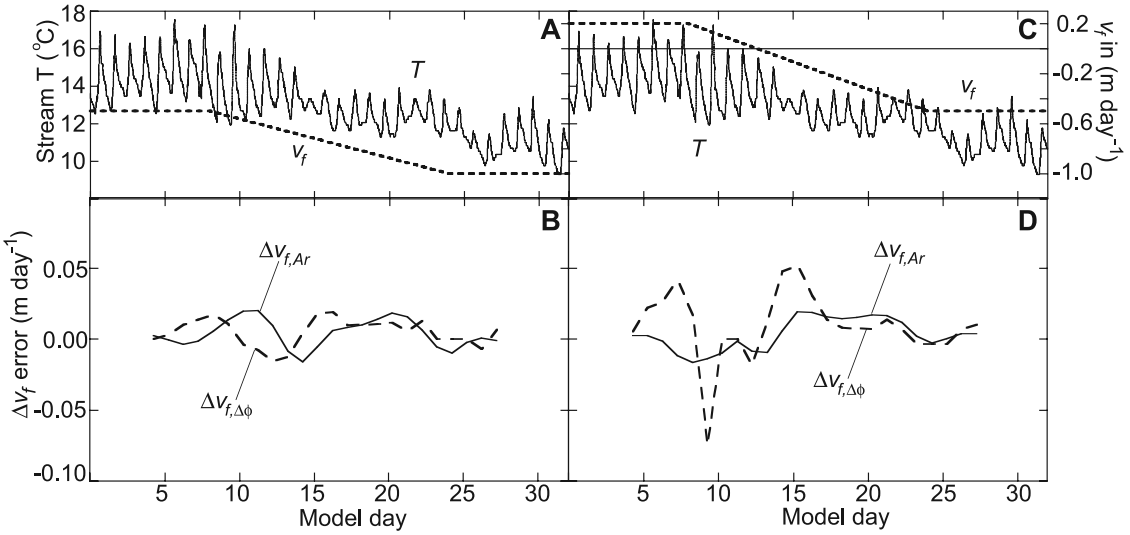

Figure 14. Numerical tests illustrating the influence of transient fluid velocities on time series method for Δz = 15 cm. (a) Stream temperature record and variable fluid seepage velocity used for boundary conditions in forward model. Velocity varied from -0.6 to -1.0 m d^{-1}. (b) Errors in seepage velocity, Δv_f, (deviations from dashed line in Figure 14a) of ±0.03 m d^{-1}. Solid lines are $\Delta v_{f,Ar}$, and dashed lines are $\Delta v_{f,\Delta\phi}$. (c) Velocity varied from 0.2 to -0.5 m d^{-1} (stream went from gaining through zero, the horizontal line, to losing). (d) Seepage velocity errors (deviations from dashed line in Figure 14c) of ±0.06 m d^{-1}.

as seepage rates change, but is not yet clear whether there is sufficient sensitivity of the analysis to these properties to allow for accurate optimization. Application of this approach to unsaturated systems would require time series estimates of saturation and saturation-dependent properties, as would forward models, but should be possible.

5. Conclusions

[43] We have developed a method for determining streambed seepage rates using time series thermal data, based on recognition that natural temperature variations in streams propagate downward into the streambed. Filtering of streambed records allows extraction of the strongest individual frequencies, facilitating interpretation of streambed temperatures to calculate seepage rates, without requiring forward modeling of coupled fluid-heat flow.

[44] The new method is based on quantifying changes in phase and amplitude of temperature variations between pairs of subsurface temperature sensors. For a reasonable range of streambed thermal properties and sensor spacings, the time series method allows reliable estimation of seepage rates of -5 to 3 m d^{-1} (-5.8×10^{-5} to 2.7×10^{-5} m s^{-1}, positive = up) based on changes in the amplitude of temperature variations, and at least ±10 m d^{-1} (±1.2 $\times$ 10^{-2} m s^{-1}) based on changes in phase. Changes in amplitude with depth are most sensitive to seepage rates under low-flow conditions, whereas variations in phase shift reach a peak in sensitivity near ±1 m d^{-1} (±1.2 $\times$ 10^{-5} m s^{-1}) and remain sensitive at much higher rates. Instrument spacing, streambed thermal parameters, and the absolute magnitude of measured temperature variations all influence applicability of the new method.

[45] Despite being based on the same physics, the new interpretive method offers several advantages in comparison to forward modeling, the approach most commonly reported in the literature. In most such modeling exercises, thermal data are used to constrain (calibrate) selected model parameters, typically including streambed hydraulic conductivity, while holding other parameters constant. The time series method has fewer data requirements, requires less setup and data handling effort, and is considerably faster. The new method is easily applied to long data sets (months to years), whereas forward modeling studies generally evaluate relatively short data sets (days to weeks). In addition, the new method requires no information on the absolute depths of temperature sensors, instead relying on the spacing between sensor pairs. This means that the method is relatively insensitive to streambed scour or sedimentation, processes that violate boundary conditions common to most forward models, allowing the method to be applied to streams and other aquatic systems under a wide range of hydrologic conditions.

[46] The new method does not bypass common limitations of using temperature measurements to estimate seepage rates, including streambed heterogeneity, finite instrument response time, and the need to estimate streambed thermal properties, and has been implemented so far only for saturated conditions. Some of these limitations can be reduced through additional method development, and by coupling this approach with forward modeling (and other approaches) where thermal and other data justify the necessary effort. When combined with independent estimates of streambed head gradients, the time series method can provide time series estimates of streambed hydraulic conductivity. The time series approach allows rapid assessment of numerous, long data sets, allowing detailed work to focus

where the effort is justified. Perhaps the greatest benefit of thermal methods in general is that they can be applied relatively easily both along and across a stream channel, providing high-resolution spatial and temporal seepage information. The time series approach may facilitate wider use of thermal methods, helping scientists and water managers to better understanding the complex temporal and spatial dynamics of surface water–groundwater interactions within aquatic systems.

Notation

A amplitude of thermal oscillation, °C.
A_r A_d/A_s, amplitude ratio; amplitude of deeper temperature record divided by shallower.
c specific heat of the sediment-fluid system, J kg^{-1} °C^{-1}.
c_f specific heat of the fluid, J kg^{-1} °C^{-1}.
f frequency, cycles s^{-1} or d^{-1}.
n porosity.
P period of thermal oscillation, $1/f$, s or d^{-1}.
T temperature °C.
t time, s.
Δt sample time interval, s or min.
v velocity of thermal front, related to fluid seepage velocity by $v = v_f/\gamma$, m s^{-1} (v_{Ar} when derived from amplitude relations, and $v_{\Delta\phi}$ when derived from phase relations).
v_f vertical fluid velocity, or seepage rate (positive = up), m s^{-1} or m d^{-1} ($v_{f,Ar}$ when derived from amplitude relations, and $v_{f,\Delta\phi}$ when derived from phase relations).
z depth, positive up, m.
Δz sensor spacing, relative depth between sensors, m.
β thermal dispersivity, m.
$\Delta\phi$ phase shift, s.
γ ratio of heat capacity of the streambed (saturated sediment-fluid system) to that of the fluid, $\gamma = \rho c/\rho_f c_f$.
κ_e effective thermal diffusivity, m^2 s^{-1}.
λ_0 baseline thermal conductivity; thermal conductivity in the absence of fluid flow, purely conductive; assumed product of geometric mean mixing between fluid ($_f$) and grains ($_g$): $\lambda_0 = \lambda_f^n \lambda_g^{(1-n)}$, W m^{-1} °C^{-1}.
λ_e effective thermal conductivity, W m^{-1} °C^{-1}.
ρ density of sediment-fluid system, kg m^{-3}.
ρ_f density of the fluid, kg m^{-3}.

[47] **Acknowledgments.** This work was funded by the U.S. Department of Agriculture (projects 2003-35102-13531 and 2002-34424-11762), the UCSC Committee on Research, and the UCSC Center for Agroecology and Sustainable Food Systems. We gratefully acknowledge Jonathan Lear and colleagues with the Pajaro Valley Water Management Agency for assistance with site access and field support. We thank Paul Hsieh for help with computer modeling. This manuscript was improved considerably by three anonymous reviewers and the associate editor.

References

Alexander, M. D., and D. Caissie (2003), Variability and comparison of hyporheic water temperatures and seepage fluxes in a small Atlantic salmon stream, *Ground Water*, *41*(1), 72–82.

Anderson, M. P. (2005), Heat as a ground water tracer, *Ground Water*, *43*(6), 1–18.

Arnell, N. W., and C. Liu (2001), Hydrology and water resources, in *Climate Change 2001: Impacts, Adaptation, and Vulnerability: Contribution of Working Group II to the Third Assessment Report of the Intergovernmental Panel on Climate Change*, pp. 194–227, Cambridge Univ. Press, New York.

Bachman, S., C. Hauge, R. McGlothlin, T. K. Parker, A. M. Saracino, and S. S. Slater (2005), *California Groundwater Management*, 272 pp., Groundwater Res. Assoc. of Calif., Sacramento.

Barlow, P. M. (1987), The use of temperature as a ground-water tracer in glacial outwash, M.S. thesis, Univ. of Ariz., Tucson.

Barnett, T. P., J. C. Adam, and D. P. Lettenmaier (2005), Potential impacts of a warming climate on water availability in snow-dominated regions, *Nature*, *438*(7066), 303–309.

Bear, J. (1972), *Dynamics of Fluids in Porous Media*, 764 pp., Elsevier, New York.

Bencala, K. E., and R. A. Walters (1983), Simulation of solute transport in a mountain pool-and-riffle stream: A transient storage model, *Water Resour. Res.*, *19*, 718–724.

Bencala, K. E., D. M. McKnight, and G. W. Zellweger (1990), Characterization of transport in an acidic and metal-rich mountain stream based on a lithium tracer injection and simulations of transient storage, *Water Resour. Res.*, *26*, 989–1000.

Bower, D., D. M. Hannah, and G. R. McGregor (2004), Techniques for assessing the climatic sensitivity of river flow regimes, *Hydrol. Processes*, *18*, 2515–2543.

Bravo, H. R., F. Jiang, and R. J. Hunt (2002), Using groundwater temperature data to constrain parameter estimation in a groundwater flow model of a wetland system, *Water Resour. Res.*, *38*(8), 1153, doi:10.1029/2000WR000172.

Bredehoeft, J. D., and I. S. Papadopulos (1965), Rates of vertical groundwater movement estimated from the Earth's thermal profile, *Water Resour. Res.*, *1*(2), 325–328.

Bredehoeft, J. D., S. S. Papadopulos, and H. H. Cooper Jr. (1982), Groundwater: The water-budget myth, in *Studies in Geophysics: Scientific Basis of Water-Resource Management*, pp. 51–57, Natl. Acad. Press, Washington, D. C.

Brigaud, F., and G. Vasseur (1989), Mineralogy, porosity, and fluid control on thermal conductivity of sedimentary rocks, *Geophys. J.*, *98*, 525–542.

Burow, K. R., J. Constantz, and R. Fujii (2005), Heat as a tracer to estimate dissolved organic carbon flux from a restored wetland, *Ground Water*, *43*(4), 545–556.

Carslaw, H. S., and J. C. Jaeger (1959), *Conduction of Heat in Solids*, 510 pp., Clarendon, Oxford, U. K.

Chen, X. H., and L. C. Shu (2002), Stream-aquifer interactions: Evaluation of depletion volume and residual effects from ground water pumping, *Ground Water*, *40*(3), 284–290.

Clark, J. F., P. Schlosser, M. Stute, and H. J. Simpson (1996), SF6-3HE tracer release experiment: A new method of determining longitudinal dispersion coefficients in large rivers, *Environ. Sci. Technol.*, *30*(5), 1527–1532.

Conant, B. (2004), Delineating and quantifying ground water discharge zones using streambed temperatures, *Ground Water*, *42*(2), 243–257.

Constantz, J., and D. A. Stonestrom (2003), Heat as a tracer of water movement near streams, in *Heat as a Tool for Studying the Movement of Ground Water Near Streams*, edited by J. Constantz and D. A. Stonestrom, *U.S. Geol. Surv. Circ.*, *1260*, 1–6.

Constantz, J., C. L. Thomas, and G. Zellweger (1994), Influence of diurnal-variations in stream temperature on streamflow loss and groundwater recharge, *Water Resour. Res.*, *30*(12), 3253–3264.

Constantz, J., M. H. Cox, and G. W. Su (2003), Comparison of heat and bromide as ground water tracers near streams, *Ground Water*, *41*(5), 647–656.

Dagan, G. (1984), Solute transport in heterogeneous porous formations, *J. Fluid Mech.*, *145*, 151–177.

de Marsily, G. (1986), *Quantitative Hydrogeology: Groundwater Hydrology for Engineers*, 440 pp., Elsevier, New York.

Gelhar, L. W., C. Welty, and K. R. Rehfeldt (1992), A critical review of data on field-scale dispersion in aquifers, *Water Resour. Res.*, *28*(7), 1955–1974.

Gillham, R. W., E. A. Sudicky, J. A. Cherry, and E. O. Frind (1984), An advection-diffusion concept for solute transport in heterogeneous unconsolidated geological deposits, *Water Resour. Res.*, *20*(3), 369–378.

Goetz, R. (2004), Stream sediment adsorption of Rhodamine-WT: Application for hydrologic tracer tests in the Pajaro River, CA, senior thesis, Univ. of Calif., Santa Cruz.

Goto, S., M. Yamano, and M. Kinoshita (2005), Thermal response of sediment with vertical fluid flow to periodic temperature variation at the surface, *J. Geophys. Res.*, *110*, B01106, doi:10.1029/2004JB003419.

Grasby, S. E., I. Hutcheon, and L. MacFarland (1999), Surface-water-groundwater interaction and the influence of ion exchange reactions on river chemistry, *Geology*, *27*, 223–226.

Greeff, G. J. (1994), Ground-water contribution to stream salinity in a shale catchment, R.S.A., *Ground Water*, *32*(1), 63–70.

Grimm, N. B., and S. G. Fisher (1984), Exchange between interstitial and surface water: Implications for stream metabolism and nutrient cycling, *Hydrobiologia*, *111*, 219–228.

Hayashi, M., and D. O. Rosenberry (2002), Effects of ground water exchange on the hydrology and ecology of surface water, *Ground Water*, *40*(3), 309–316.

Healy, R. W. (1990), Simulation of solute transport in variably saturated porous media with supplemental information on modifications to the U.S. Geological Survey's computer program VS2D, *U.S. Geol. Surv. Water Resour. Invest. Rep., 90-4025*, 125 pp.

Healy, R. W., and A. D. Ronan (1996), Documentation of computer program VS2DH for simulation of energy transport in variably saturated porous media; modification of the U. S. Geological Survey's computer program VS2DT, *U.S. Geol. Surv. Water Resour. Invest. Rep.*, *96-4230*, 36 pp.

Hendricks, S. P., and D. S. White (1991), Physicochemical patterns within a hyporheic zone of a northern Michigan river, with comments on surface-water patterns, *Can. J. Fish. Aquat. Sci.*, *48*(9), 1645–1654.

Hopmans, J. W., J. Simunek, and K. L. Bristow (2002), Indirect estimation of soil thermal properties and water flux using heat pulse probe measurements: Geometry and dispersion effects, *Water Resour. Res.*, *38*(1), 1006, doi:10.1029/2000WR000071.

Horai, K. (1971), Thermal conductivity of rock-forming minerals, *J. Geophys. Res.*, *76*, 1278–1308.

Hsieh, P. A., W. Wingle, and R. W. Healy (2000), VS2DI—A graphical software package for simulating fluid flow and solute of energy transport in variably saturated porous media, *U.S. Geol. Surv. Water Resour. Invest. Rep.*, *99-4130*, 16 pp.

Ingebritsen, S. E., and W. E. Sanford (1998), *Groundwater in Geologic Processes*, 341 pp., Cambridge Univ. Press, New York.

Kilpatrick, F. A., and E. D. Cobb (1985), Measurement of discharge using tracers, *U.S. Geol. Surv. Tech. Water Resour. Invest. Rep., Book 3, Chap. A16*, 52 pp.

Kinoshita, M. (1994), Estimation of grain thermal conductivity in the turbidite sediment of the Juan de Fuca Ridge, *Proc. Ocean Drill. Program Sci. Results*, *139*, 553–558.

Lapham, W. W. (1989), Use of temperature profiles beneath streams to determine rates of vertical ground-water flow and vertical hydraulic conductivity, pp. 35.

Lee, D. R., and J. A. Cherry (1978), A field exercise on groundwater flow using seepage meters and mini-piezometers, *J. Geol. Ed.*, *27*(1), 6–10.

Leibundgut, C., U. Speidel, and H. Wiesner (1993), Transport processes in rivers investigated by tracer experiments, in *Tracers in Hydrology*, edited by N. E. Peters et al., *IAHS Publ.*, *215*, 211–217.

Lettenmaier, D. P., A. W. Wood, R. N. Palmer, E. F. Wood, and E. Z. Stakhiv (1999), Water resources implications of global warming: A U.S. regional perspective, *Clim. Change*, *43*, 537–579.

Malard, F., K. Tockner, M.-J. Dole-Olivier, and J. V. Ward (2002), A landscape perspective of surface–subsurface hydrological exchanges in river corridors, *Freshwater Biol.*, *47*, 621–640.

Mansure, A. J., and M. Reiter (1979), A vertical groundwater movement correction for heat flow, *J. Geophys. Res.*, *84*, 3490–3492.

Neuman, S. P. (1990), Universal scaling of hydraulic conductivities and dispersivities in geologic media, *Water Resour. Res.*, *26*(8), 1749–1758.

Neuman, S. P. (1995), On advective transport in fractal permeability and velocity-fields, *Water Resour. Res.*, *31*(6), 1455–1460.

Niswonger, R., and D. E. Prudic (2003), Modeling heat as a tracer to estimate streambed seepage and hydraulic conductivity, in *Heat as a Tool for Studying the Movement of Ground Water Near Streams*, edited by J. Constantz and D. A. Stonestrom, *U.S. Geol. Surv. Circ.*, *1260*, 81–89.

Panagoulia, D., and G. Dimou (1996), Sensitivities of groundwater-stream-flow interaction to global climate change, *Hydrol. Sci. J.*, *41*(5), 781–796.

Petts, G. E., M. A. Bickerton, C. Crawford, D. N. Lerner, and D. Evans (1999), Flow management to sustain groundwater-dominated stream ecosystems, *Hydrol. Processes*, *13*, 497–513.

Power, G., R. S. Brown, and J. G. Imhof (1999), Groundwater and fish - insights from northern North America, *Hydrol. Processes*, *13*, 401–422.

Ronan, A. D., D. E. Prudic, C. E. Thodal, and J. Constantz (1998), Field study and simulation of diurnal temperature effects on infiltration and variably saturated flow beneath an ephemeral stream, *Water Resour. Res.*, *34*(9), 2137–2153.

Rosenberry, D. O., and R. H. Morin (2004), Use of an electromagnetic seepage meter to investigate temporal variability in lake seepage, *Ground Water*, *42*(1), 68–77.

Ruehl, C., A. T. Fisher, C. E. Hatch, G. Stemler, M. Los Huertos, and C. Shennan (2006), Differential gauging and tracer tests resolve seepage fluxes in a strongly-losing stream, *J. Hydrol.*, doi:10.1016/j.jhydrol.2006.03.025, in press.

Sass, J. H., A. H. Lachenbruch, and R. J. Munroe (1971), Thermal conductivity of rocks from measurements on fragments and its application to heat-flow determinations, *J. Geophys. Res.*, *76*, 3391–3401.

Shao, M., R. Horton, and D. B. Jaynes (1998), Analytical solution for one-dimensional heat conduction-convection equation, *Soil Sci. Soc. Am. J.*, *62*, 123–128.

Silliman, S. E., and D. F. Booth (1993), Analysis of time-series measurements of sediment temperatures for identification of gaining vs. losing potions of Juday Creek, Indiana, *J. Hydrol.*, *146*, 131–148.

Silliman, S. E., J. Ramirez, and R. L. McCabe (1995), Quantifying downflow through creek sediments using temperature time series—One-dimensional solution incorporating measured surface temperature, *J. Hydrol.*, *167*, 99–119.

Smith, L., and D. S. Chapman (1983), On the thermal effects of groundwater flow. 1. Regional scale systems, *J. Geophys. Res.*, *88*, 593–608.

Smith, R. L. (1986), Freshwater ecosystems, in *Elements of Ecology*, edited by R. L. Smith, pp. 552–579, HarperCollins, New York.

Snyder, M. A., J. A. Bell, L. C. Sloan, P. B. Duffy, and B. Govindsamy (2002), Climate responses to a doubling of atmospheric carbon dioxide for a climatically vulnerable region, *Geophys. Res. Lett.*, *29*(11), 1514, doi:10.1029/2001GL014431.

Sophocleous, M. (2000), From safe yield to sustainable development of water resources—The Kansas experience, *J. Hydrol.*, *235*, 27–43.

Sophocleous, M. (2004), Climate change: Why should water professionals care?, *Ground Water*, *42*(5), 637.

Stallman, R. W. (1965), Steady one-dimensional fluid flow in a semi-infinite porous medium with sinusoidal surface temperature, *J. Geophys. Res.*, *70*, 2821–2827.

Stonestrom, D. A., and K. W. Blasch (2003), Determining temperature and thermal properties for heat-based studies of surface-water ground-water interactions, in *Heat as a Tool for Studying the Movement of Ground Water Near Streams*, edited by J. Constantz and D. A. Stonestrom, *U.S. Geol. Surv. Circ.*, *1260*, 73–78.

Sudicky, E. A., J. A. Cherry, and E. O. Frind (1983), Migration of contaminants in groundwater at a landfill: A case study, *J. Hydrol.*, *63*, 81–108.

Taniguchi, M. (1993), Evaluation of vertical groundwater fluxes and thermal-properties of aquifers based on transient temperature-depth profiles, *Water Resour. Res.*, *29*(7), 2021–2026.

Valett, H. M., J. A. Morrice, C. N. Dahm, and M. E. Campana (1996), Parent lithology, surface-groundwater exchange, and nitrate retention in headwater streams, *Limnol. Oceanogr.*, *41*(2), 333–345.

Winter, T. C., J. W. Harvey, O. L. Franke, and W. M. Alley (1998), Ground water and surface water: A single resource, *U.S. Geol. Surv. Circ.*, *1139*, 79 pp.

Woessner, W. W. (2000), Stream and fluvial plain ground water interactions: Rescaling hydrogeologic thought, *Ground Water*, *38*(3), 423–429.

Woodbury, A. D., and L. Smith (1985), On the thermal effects of 3-dimensional groundwater-flow, *J. Geophys. Res.*, *90*, 759–767.

Woodside, W., and J. H. Messmer (1961), Thermal conductivity of porous media. I. Unconsolidated Sands, *J. Appl. Phys.*, *32*(9), 1688–1706.

Xu, M. J., and Y. Eckstein (1995), Use of weighted least-squares method in evaluation of the relationship between dispersivity and field-scale, *Ground Water*, *33*(6), 905–908.

J. Constantz, U.S. Geological Survey, 345 Middlefield Rd, MS 496, Menlo Park, CA 94025, USA.

A. T. Fisher, C. E. Hatch, and C. Ruehl, Earth and Planetary Sciences Department, University of California, E&MS A232, 1156 High Street, Santa Cruz, CA 95064, USA. (chatch@ucsc.edu)

J. S. Revenaugh, Department of Geology and Geophysics, University of Minnesota, Minneapolis, MN 55455, USA.